Modeling and Experimental Verification of the Dynamics of Rigid and Flexible Pendulums

Ashish Mohan[1], S. K. Saha[2], S. P. Singh[3], D. Jaitly[4]

[1]Project Scientist and Research Scholar [2,3]Assoc. Prof. [4]Technical Assistant [2]Communicating author
Dept. of Mechanical Engg, Indian Institute of Technology Delhi, New Delhi-110016
[1]ashishsept13@rediffmail.com [2] saha@mech.iitd.ernet.in

Abstract: Dynamic modeling methodology of a mechanical system consisting of both rigid and flexible links is presented in this paper. The model is based on the hybrid formulation of rigid-body systems, as proposed earlier by the authors. Using the Euler-Lagrange equations of motion and the properties of Decoupled Natural Orthogonal Complement (DeNOC) matrices, it is shown that the resultant dynamic equations are equivalent to those obtained from the Newton-Euler equations. Hence the term 'hybrid' formulation was used. In this paper, the methodology is used to accommodate flexible bodies also. To illustrate the concept, modeling of a single-link system under gravity, i.e., a pendulum has been carried by considering it both rigid and flexible. Experiments were conducted, where joint angles were detected using potentiometer and the link deflections using strain-gauges. Damping of the joint was calculated from the experiment and added to the theoretical model. Both the simulation and experimental results are then compared

Keywords: *Dynamic modeling, Hybrid formulation, DeNOC, Experimental results*

1 INTRODUCTION

Research on robot arms with flexible links and its control started in the international arena since early 1970s. A comprehensive review of the various techniques of modeling flexible robotic arms is given in [1]. Different methods for determination of the dynamic models of the multibody systems may be principally distinguished into two categories: those based on the scalar approach of Euler-Lagrangian (EL) formulation, and the others based upon vectorial Newton-Euler (NE) formulation. The EL formulation requires successive differentiation of algebraic functions of the kinetic and potential energies of the system at hand. These require complicated partial differentiations for complex multibodies. Alternatively, NE equations of motion require the computation of reaction forces and moments at the joints which do not contribute to the motion of the system at hand. However, using the concept of orthogonal complements, e.g., in [2], the NE equations can be reduced to a set of independent equations of motion free from the reactions. In this paper, a recursive algorithm for the forward dynamics of flexible robotic manipulators based on the decoupled natural orthogonal complement (DeNOC) matrices is presented. Forward dynamics is defined as the determination of the joint angles, rates from the numerical integrations of the joint accelerations solved from a set of dynamic equations of motion while the external torques and forces are known. Additional advantages of the use of the DeNOC matrices are as follows:

1)They provide the expression of elements of the matrices associated with the dynamic equations of motion in analytical recursive form; 2) Many physical interpretations of different terms appear in the intermediate steps to derive the equations of motion, for example, the mass matrix of composite body, etc; 3) Recursive algorithms for both inverse and forward dynamics are possible.

Dynamics of multi-link flexible manipulators are highly non-linear as the vibrational frequencies of these robots are configuration dependent. Furthermore, external factors such as friction, joint damping, working environment of robot, etc., cannot be accurately modeled without complex calculations and reasonable assumptions. As such it becomes necessary to complement the theoretical studies with the experimental observations for accurate dynamic analysis of the flexible multilink robotic systems. Extensive experimental works on determination of the response of flexible manipulators are reported in the literature [3-6]. Shuzhi,

Lee and Zhu [3] have studied the strain feedback of a single-link flexible manipulator for improving its regulation. Results using strain gages and accelerometers as encoder devices have also been reported [4-5]. In this paper, results of a series of experiments conducted at the Mechatronis Lab., IIT Delhi on a single rigid and flexible link pendulums are reported. A comparision of the proposed theoretical model and the experimental results is carried out. The paper is organized as follows: In Section 2, the dynamic modeling methodology using the DeNOC matrices is presented whereas Section 3 presents the dynamic modeling of rigid and flexible pendulums. Section 4 presents the details of the experimental set-up, whose results are given in Section 5. Finally the conclusions are given in Section 6.

2 DYNAMIC MODELING USING THE DENOC

Figure 1 shows a serial system having a fixed base, and consisting of n_r rigid and n_f flexible links.

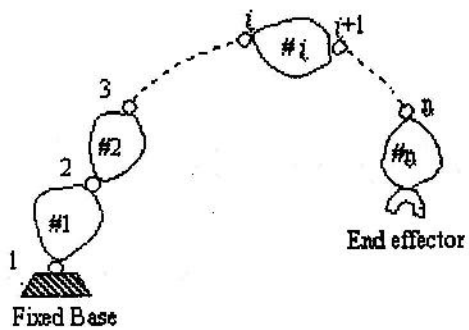

Fig. 1. An n-link serial robotic system

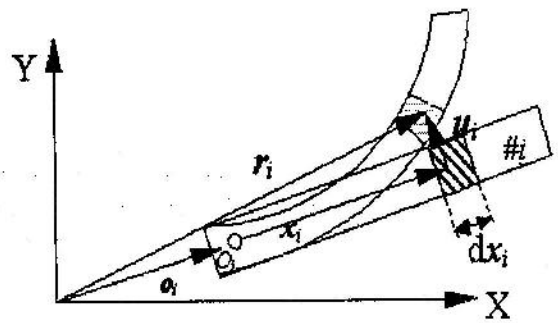

Fig. 2 The i^{th} flexible link and the elemental length, dx_i

Each flexible link is assumed to vibrate in 'm' modes. The total number of moving links in the robot is then, $n=n_f+n_r$. Now, the kinetic energy for each link, say, the i^{th} one, denoted by, T_i, is given by

$$T_i = \frac{1}{2}\int_0^{l_i} \rho_i \dot{r}_i^T \dot{r}_i dx_i + T_{hi} + T_{pi} \tag{1}$$

where ρ_i is the mass per unit length of the i^{th} link, and $\mathbf{r}_i$ is the position vector of any small element in the link after it is deflected from the rigid position, as indicated in Fig 2. The terms T_{hi} and T_{pi} are respectively the kinetic energies due to hub and the payload on the i^{th} link. The total kinetic energy of the whole system is then obtained as, $T = \sum_{i=1}^{n} T_i$ Next, the EL equations of motion of the system at hand can be obtained as

$$\frac{d}{dt}\left(\frac{\partial T}{\partial \dot{q}_i}\right) - \frac{\partial T}{\partial q_i} = \tau_i \qquad \dot{q}_i \equiv \left[\dot{\theta}_i \quad \dot{b}_{i1} \quad \cdots \quad \dot{b}_{im}\right]^T \tag{2}$$

for $i=1, \ldots, n$ where $\dot{q}_i$ is the $(1+m)$-dimensional vector of the independent generalized rates of link i, θ_i is the displacement of the i^{th} joint and b_{ik} is the time dependent amplitude variable at the k^{th} mode. Moreover, τ_i is the (1+m)-dimensional vector of generalized forces due to gravity, strain energy and the external forces and moments on the i^{th} link. Furthermore using the hybrid formulation proposed in [6], eq. (2) can be shown to be equivalent to

$$N_d^T N_l^T \hat{\dot{w}} = \tau \tag{3}$$

where $\hat{w} \equiv \left[\hat{w}_1^T \quad \cdots \quad \hat{w}_n^T\right]^T$ is the $\hat{n} \equiv 6n_r + (6+m)n_f$ dimensional vector and $\tau \equiv \left[\tau_1^T \quad \cdots \quad \tau_2^T\right]^T$ is the $\bar{n} \equiv 6n_r + (6+m)n_f$ dimensional vector, whereas the $\hat{n} \times \hat{n}$ lower triangular matrix N_l and the $\hat{n} \times \bar{n}$ block diagonal matrix, N_d, are the DeNOC matrices of the flexible body manipulator similar to those corresponding to the rigid body system [2]. Equation (3) will be illustrated with the help of a single flexible link arm in subsection 3.2.

3. DYNAMIC MODELING OF PENDULUMS

In this section, dynamic modeling of a single link rigid and flexible arm, namely the pendulum system, is carried out whose results will be compared with those available from the experiments.

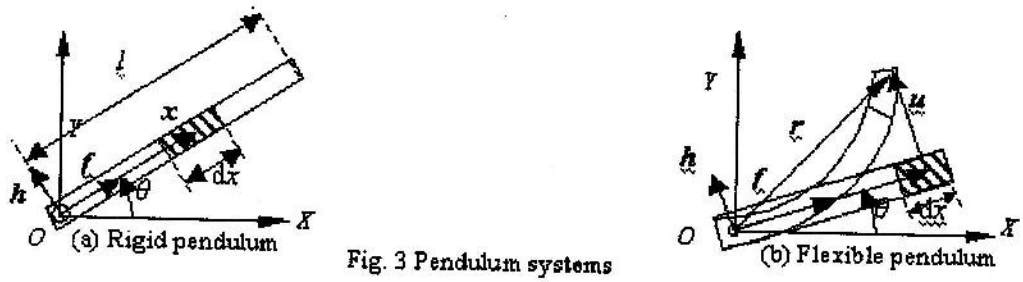

Fig. 3 Pendulum systems

3.1 Rigid Pendulum

For the rigid pendulum as shown in Fig. 3(a), first the 6-dimensional vector, $\hat{w}$ of eq. (3) [6] is written as,

$$\hat{w} \equiv \int_0^l \rho \begin{bmatrix} \ddot{r}^T & (x \times \ddot{r})^T \end{bmatrix}^T dx \tag{4}$$

Where $\ddot{r} \equiv \ddot{x}$ as the origin of the link coincides with that of the reference frame. Vector $\ddot{r}$ or $\ddot{x}$ is the acceleration of the elemental link dx shown in Fig. 3(a), which is expressed as $\ddot{r} \equiv \ddot{x} = \dot{\omega} \times x + \omega \times (\omega \times x) = \ddot{\theta} x h$ in which $\omega \times (\omega \times x) = 0$ as the motion is planer. Moreover, $\ddot{\theta}$ is the joint acceleration, x is the magnitude of the vector, x, and h is the unit vector orthogonal to the unit vector f along x. The term $x \times \ddot{r}$ is now obtained as $x \times \ddot{r} = \ddot{\theta} x^2 f \times h = \ddot{\theta} x^2 e$. The unit vector e is parallel to the axis of the revolute joint coupling the link with the ground, i.e. fixed frame. Equation (4) is then obtained as

$$\hat{w} = \rho \ddot{\theta} \begin{bmatrix} h \\ l^2 e/3 \end{bmatrix} \tag{5}$$

In order to obtain eq. (3) the DeNOC matrices are obtained next. Note that for the single rigid-link system, the matrix N_i is identity, whereas the matrix $N_d \equiv p - p \equiv \begin{bmatrix} 0^T & e^T \end{bmatrix}^T$ being the 6-dimensional joint-motion vector [2]. Equation (3) is then obtained as,

$$\rho \ddot{\theta} \begin{bmatrix} 0^T & e^T \end{bmatrix} \begin{bmatrix} h \\ l^2 e/3 \end{bmatrix} = \rho l^3 \ddot{\theta}/3 \tag{6}$$

Hence the equation of motion for the rigid pendulum can be given by $\frac{\rho l^3}{3} \ddot{\theta} = \tau$ where is the external torque causing the motion. In the case of pendulum, $\tau \equiv \rho l^2 g \cos\theta - g$ being the acceleration due to gravity. In the presence of hub inertia I_h, payload m_p and damping, the eq. (6) is modified as

$$\left(\frac{\rho l^3}{3} \ddot{\theta} + m_p l^2 + I_h \right) \frac{\rho l^3}{3} \ddot{\theta} + \xi \dot{\theta} = \rho l^2 g \cos\theta + m_p g l \cos\theta \tag{7}$$

where ξ is the damping coefficient, which will be obtained from experiments as explained in Section 4.

3.2 Flexible Pendulum

Similarly for the flexible pendulum, as shown in Fig. 3(b), the link is assumed to vibrate in its first mode only. First, the 7-dimensional vector, of eq. (3), is written as

$$\hat{w} \equiv \int_0^l \rho \begin{bmatrix} \ddot{r}^T & (r \times \ddot{r})^T & \ddot{r}^T \lambda \end{bmatrix}^T dx \; ; \; u = \lambda^T b \tag{8}$$

where $\boldsymbol{r} \equiv \boldsymbol{x} + \boldsymbol{u}$ and $\boldsymbol{u}$ is the deflection of the small element dx on the link, as shown in Fig. 3(b), λ is the vector of shape functions associated with vibrations in first mode. It is given by $\lambda \equiv [0 \quad s \quad 0]^T$, in which 's' is the shape function associated in the X-Y plane of the link. Moreover, $\boldsymbol{b} \equiv [0 \quad b \quad 0]^T$ is the vector of vibration amplitudes which is a function of time. Vector $\ddot{\boldsymbol{r}}$ is the acceleration of the dx expressed as, $\ddot{\boldsymbol{r}} \equiv \dot{\boldsymbol{\omega}} \times \boldsymbol{r} + 2\boldsymbol{\omega} \times \dot{\boldsymbol{u}}^l + \lambda \ddot{\boldsymbol{u}}^l + \boldsymbol{\omega} \times (\boldsymbol{\omega} \times \boldsymbol{r})$ in $\dot{\boldsymbol{u}}^l \equiv [0 \quad s\dot{b} \quad 0]^T$ which represents the component of the vector $\dot{\boldsymbol{u}}$ due to its change in the local coordinate frame, i.e., the one indicated with the unit vectors, $\boldsymbol{f}$ and $\boldsymbol{h}$ shown in Fig. 3(b). Also, $\boldsymbol{\omega} \times (\boldsymbol{\omega} \times \boldsymbol{r}) = 0$ as the motion is planer. In order to obtain eq. (3) the DeNOC matrices are btained next. Note that for the single flexible-link system, the matrix N_l is identity, whereas the matrix $N_d \equiv \boldsymbol{P} - \boldsymbol{P} \equiv \begin{bmatrix} \boldsymbol{0}^T & \boldsymbol{e}^T & 0 \\ \boldsymbol{0}^T & \boldsymbol{0}^T & 1 \end{bmatrix}^T$ being the 7×2 joint cum flexibility propagation matrix. The left hand side of eq. (3) is then obtained as $\begin{bmatrix} \boldsymbol{0}^T & \boldsymbol{e}^T & 0 \\ \boldsymbol{0}^T & \boldsymbol{0}^T & 1 \end{bmatrix} \begin{bmatrix} \ddot{\boldsymbol{r}} \\ (\boldsymbol{x}+\boldsymbol{u}) \times \ddot{\boldsymbol{r}} \\ \lambda^T \ddot{\boldsymbol{r}} \end{bmatrix} = \begin{bmatrix} \boldsymbol{e}^T [(\boldsymbol{x}+\boldsymbol{u}) \times \ddot{\boldsymbol{r}}] \\ \lambda^T \ddot{\boldsymbol{r}} \end{bmatrix}$ (9)

Hence the equations of motion for the flexible pendulum is given by $\rho(\frac{l^3\ddot{\theta}}{3} + S_1 b^2 \ddot{\theta} + S_2 \ddot{b} + 2S_1 b\dot{\theta}\dot{b}) = \tau_1$ and $\rho(S_2\ddot{\theta} + S_1\ddot{b} - 2S_1 b\dot{\theta}^2) = \tau_2$, where τ_1 and τ_2 are the external generalized forces, and S_1 and S_2 are the values of the shape functions evaluated over the length of link, i.e., $S_1 \equiv \int_0^l s^2 dx$ and $S_2 \equiv \int_0^l xs dx$. Including the hub inertia I_h, payload m_p, and damping the equations of pendulum moving due to gravity only, i.e. $\tau_1 \equiv \rho l^2 g \cos\theta$ and $\tau_2 = 0$, become

$$\rho[l^3/3 + S_1 b^2 + m_p(l^2 + S_3^2 b^2) + I_h]\ddot{\theta} + (S_2 + m_p l S_3)\ddot{b} + 2(S_1 + S_3^2) b\dot{\theta}\dot{b} + \xi\dot{\theta} = \rho l^2 g \cos\theta - m_p g l \cos\theta$$

$$\rho(S_2 + m_p l S_3)\ddot{\theta} + (S_1 + m_p S_3^2)\ddot{b} - (2S_1 + m_p S_3^2) b\dot{\theta}^2 + \xi_m \dot{b} = 0 \qquad (10)$$

where $S_3 \equiv s(l)$, ξ is the joint damping coefficient and ξ_m is the modal damping coefficient for vibrations.

4. EXPERIMENTAL SET-UP

Objective of our experiments is to validate the theoretical results obtained using eqs. (7) and (10). In both the cases, i.e., rigid and flexible, the pendulums are dropped from different heights. For flexible arm the deflection at the tip is also measured besides the joint rotation. In the first part of experiments, the angular displacement of the link using a wire-pot potentiometer, mounted at the joint while it is dropped from different heights is measured. The output of the potentiometer is also verified using a 20g accelerometer mounted at the tip of the rigid link. The experimental set-up is shown in Fig. 4. Building on the results of the experiments on the rigid pendulum, the second part of the experiments is carried out to find the position of the tip of the flexible pendulum. It has two components, namely, the displacement due to the joint motion of the link under gravity, and the link displacement due to its flexibility. Since the joint motion oscillations and the tip vibrations occur at different frequencies two separate transducers are used to measure the above two components. In the present set-up, as shown in Fig. 5, the joint motion of the flexible-link is measured using the same wire-pot potentiometer as used in the rigid pendulum. The deflection in the tip position is measured using strain-gauges mounted at the root of the link. The strain produced at the root of the link due to its bending in the lateral direction is calibrated to get the magnitude of the tip deflection. Two strain gauges are mounted on each side of the link so that the proper conditioning of the

readings gives the direction of the deflection. The experimental results are then compared with those obtained using eq. (10). Note that the actual behaviors of the pendulums clearly indicate the joint damping which is incorporated in the theoretical model by assuming its behavior linear. Moreover, the lumped inertia due to potentiometer is included as the hub inertia and the mass of accelerometer is taken as a payload at the tip of link. The damping coefficient is obtained from the decay curve of amplitude [7], namely, $\xi = \eta\xi_c$; η is the ratio of the successive amplitudes of oscillations and ξ_c is the critical damping coefficient given by $\xi_c = \rho l^2\sqrt{2lg/3}$.

4.1 Equipments Used

Figures 4(a)-(b) show the photograph and schematic diagram of the experimental set-up for the measurement of the joint angle of rigid pendulum. Bourns: $10\,K\Omega, \pm 25\%$ linearity, wire-wound potentiometer, and a 20g accelerometer are used. The physical parameters of the link are shown in Table 1. When the accelerometer is used to measure the joint motions the output is amplified using a Bruel and Kjaer charge amplifier (Type: 2635; Lower frequency cut-off: 2Hz; Higher frequency cut-off: 30Hz; and Calibration factor: 100mV/mm). The charge sensitivity and voltage sensitivity of the charge amplifier are $1.003pC/ms^{-2}$ and $0.88mV/ms^{-2}$ respectively. The output of charge amplifier and the wire-bound potentiometer are given to pico-virtual CRO, having a interface with Pentium IV Intel processor computer. Note here that the joint motion using accelerometer fitted at the tip of the link is obtained as follows: The charge amplifier is set to displacement mode which would provide arc distance of the tip where the accelerometer is fitted. Dividing the arc by the pendulum length gives the joint angle.

Figures 5(a)-(b) similarly show the experimental set-up for the joint-motion and tip deflection measurements of the flexible pendulum whose physical parameters are given in Table 1. For calibration the link is clamped horizontally and its tip is made deflected by increasing the load on it through a load-cup. The corresponding change in the output voltage is then recorded on a sanwa DMM, PC5000digital multimeter of 0.01 resistance and 0.01mV resolution. The strain-gauge signal is amplified using an ADAM-3016, DIN rail-mounted amplifier module connected to a 1000DC Volts, 3-way isolation between input, output and power supply. The calibration curve of the circuit shows a straight-line behavior. Here a Bourns: $10\,K\Omega, \pm 25\%$ linearity, wire-wound,10-turn wire-pot potentiometer is used at the joint for better resolution of joint angle measurement. In order to measure the tip deflection due to the link flexibility four strain-gauges are put at the root of the link close to the joint, as shown in location 2 of Fig. 5(a)-(b).

5. RESULTS

In this section the results of experiments on rigid and flexible link pendulums are produced. First, the experimental results for a single rigid pendulum are presented and compared with the simulation results based on eq. (7) solved using ode45 function of Matlab 6.5. Then, the results for flexible pendulum are presented and compared with the simulation results obtained from eq. (10).

5.1 Rigid Pendulum

Figure 6(a) shows the experimental plot of joint angle obtained from the wire-pot potentiometer when the rigid link is falling freely under gravity from horizontal position, i.e., $\theta = 180^\circ$ Figure 6(b) shows the same result, i.e., the joint angle, using a 20g accelerometer when the link's initial position is 7 degrees in anticlockwise direction from its vertical position, i.e., $\theta = -97^\circ$ .Since an accelerometer works correctly in a linear motion the angle of the pendulum from the vertical position is kept fairly small, i.e., 7°, so that the motion is almost straight line providing correct results. This aspect has been checked by measuring the results from the accelerometer when the link is dropped from $\theta = 0^\circ$. It was not giving correct results. From Fig. 6(a) the frequency of the oscillation obtained from the experiments using potentiometer is 0.9Hz, whereas the frequency obtained from the theoretical formulation is 0.88Hz. The results match closely. For the calculation of damping coefficient, ξ of eq. (7), experimental results of Fig. 6(a) or (b) are used and linear damping is assumed. The value obtained for ξ using the equation provided before Subsection 4.1

as, $\xi = 1.9\times10^{-3}$ Nms. Equation (7) is now used to obtain the simulation results using ode45 of Matlab. The amplitude of oscillation matches closely upto 7 seconds before the results start deviating due to actual non-linear effect of damping. The experimental results using the accelerometer, also match closely with the simulation results as indicated in Fig. 6(b). However, since present work is conducted at moderate speeds (maximum $\dot{\theta} = 0$ rad/s) the charge build-up characteristics of charge amplifier become prominent and the accuracy of results is not as good as with the potentiometer. Moreover, the accelerometer cannot be used for large angles of rotation. Hence a wire-pot potentiometer with higher resolution is used to find the joint displacement of the flexible pendulum.

Table 1: Physical parameters of the link

Link	Material	Length (m)	Cross section (m^2)	Mass(Kg)	Hub Inertia (Kgm^2)	Payload (Kg)
Rigid	Carbon steel	0.30	0.018×0.004	0.180	2×10^5	0.020
Flexible	Spring steel	0.30	0.025×0.002	0.60	2×10^5	0

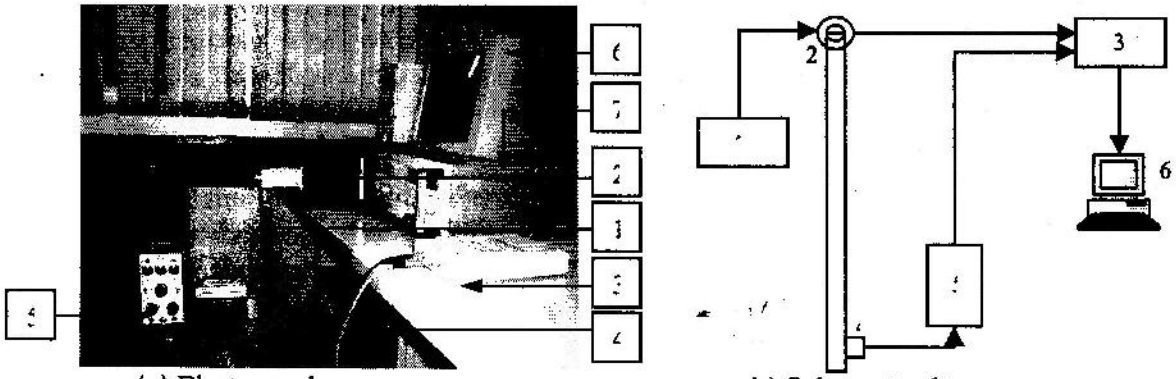

(a) Photograph b) Schematic diagram

1. Rigid link; 2. Wire-pot; 3. Pico CRO; 4. Accelerometer; 5. Charge amplifier; 6. Computer; 7. Power supply

Fig. 4 Experimental set-up for rigid pendulum

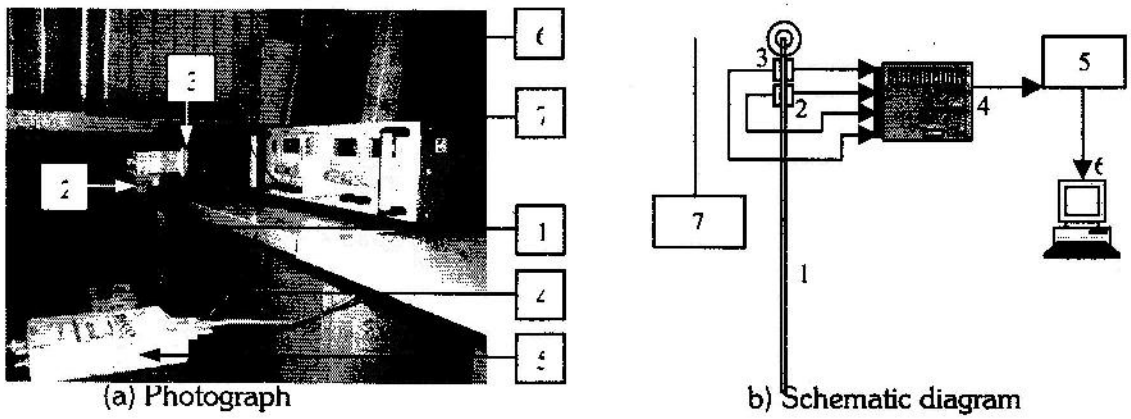

(a) Photograph b) Schematic diagram

1. Flexible link; 2. Strain-gauge; 3. Wire-pot; 4. Amplifier; 5. Pico-CRO; 6. Computer;7. Power supply

Fig. 5 Experimental set-up for flexible pendulum

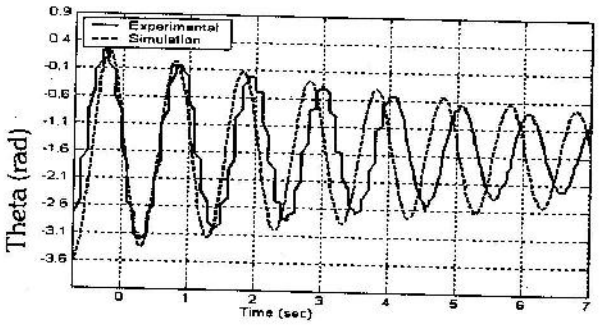

(a) Initial position $\theta = -180°$

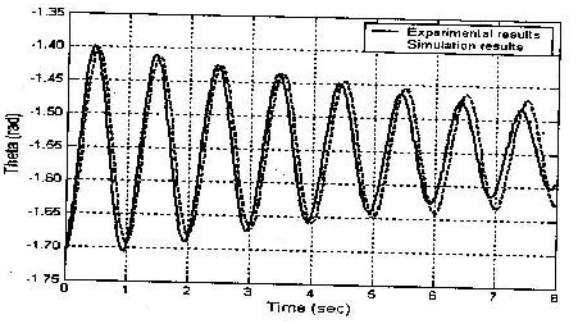

(a) Initial position $\theta = -97°$

Fig. 6 Comparison of results for rigid-pendulums

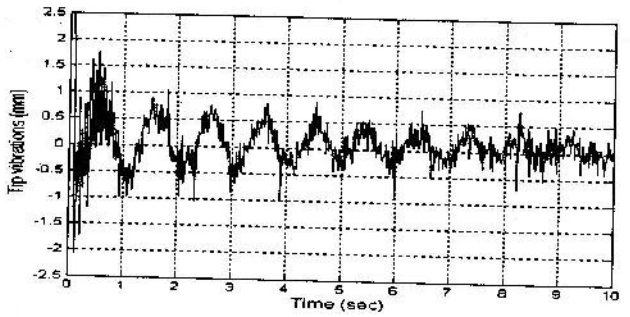

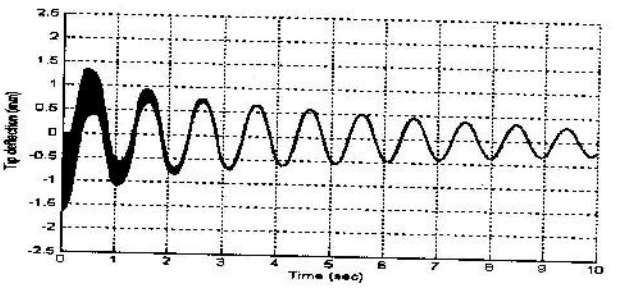

(a) Experimental results (b) Simulation results

Fig. 7 Tip Deflections of flexible pendulums

5.2 Flexible Pendulum

In this section, experimental results for the single flexible pendulum falling freely under gravity from the horizontal position, i.e., $\theta = 0^0$, with no initial deflection are presented. Since the joint angle results are same as those for the rigid pendulum they are not reported. Figures 7(a)-(b) show the experimental and simulation results while the link is released from the horizontal position and falling freely due to gravity. The tip vibrations due to flexibility are the high frequency peaks while the joint motion oscillation is the lower frequency curve. Moreover, the vibrations are more prominent in the initial cycles of oscillation. Also, the rate of damping of the amplitude of vibrations due to flexibility is also different than the joint damping. The damping in amplitude of vibrations due to flexibility is referred as model damping in the literature [7]. In order to analyze the tip vibrations and joint oscillations, these frequencies can be segregated using Fourier transformation or frequency filters. From Fig. 7(a), the oscillation frequency is obtained to be 1.1Hz, whereas the Fourier transformation of the experimental results, i.e. Fig. 7(a), the tip vibration frequency is 35Hz. From the simulation plots in Fig. 7(b), the oscillation frequency is also 1.1Hz whereas the vibration frequency is 35.5Hz. Hence, the proposed model for the flexible beam is validated. For the verification of the tip vibration, an analytical formula [7], $\omega_n = \beta^2 \sqrt{EI/\rho}$, – β,E, I and ρ being the numerical constant depending upon the mode of vibration, link configuration, elasticity modulus of link, moment of inertia of the cross section of link about its axis, and the mass per unit length of link, respectively-which gives 35Hz. A quick experiment on the flexible link has been conducted to calculate its natural frequency as well. For this, the tip of the link is displaced by hitting it mildly using a mallet. The link is allowed to vibrate under its natural condition which is recorded and the natural frequency of the flexible link is obtained as 37Hz, which closely matches with that obtained analytically and the free fall simulation of the flexible pendulum. In the paper, linear damping characteristics is assumed for theoretical model. Hence, the experimental results start deviating from the simulation results when the non-linear characteristics of the joint damping become prominent.

6. CONCLUSIONS

Dynamic model of serial flexible link robot arm has been formulated using DeNOC matrices. Even though the modeling is shown for n-link serial manipulators and suitable for recursive numerically stable forward dynamics algorithms, it is illustrated with a simple single-link pendulum systems. In order to verify the simulation results, a series of experiments were performed while the pendulum is dropped from different angles. The experimental results are matching with those obtained from the simulations based on the dynamic model. It is seen that the joint motion of the flexible link converges at a lower frequency as compared to the elastic tip vibrations. The experimental results are also highly sensitive to the characteristics of the position transducers used. This difference is prominent in the case of rigid-link pendulum wherein charge build-up characteristics of charge amplifier associated with accelerometer leads to delay in reaching steady state of the transducer. The accelerometers cannot be used for measuring the angular displacement of the links dropping from large angles, because these sensors are based on linear accelerations. Hence, potentiometer and strain gauges are used to measure the joint-angle and tip-position of the flexible pendulum. The strain-gauge set-up used has linear characteristics. However since the resistance of the strain gauges is highly dependent on temperature, the experiments have to be carried out in controlled environments. The contributions of the paper are highlighted as follows: 1) Exposure to a new dynamic modeling methodology for a flexible robotic system; 2) Illustration of the above methodology using one-link rigid and flexible arms; 3) Simulation using the Matlab; 4) Performing experiments to measure the joint angles and the tip deflection for the flexible link falling under gravity, hence, the term pendulum is used in paper; 5) Interpretation and validation of both the simulation and experimental results.

ACKNOWLEDGEMENTS

The research work reported in this paper is carried out under the financial aid from the DST, Government of India (SR/S3/RM/46/2002) which is duly acknowledged. The help extended by Mr. Subhasis Pati, a student of M. Tech in the Mechanical Engineering Department of IIT Delhi is also acknowledged.

REFERENCES

[1] Shabana, A. A., "Flexible multibody dynamics: Review of past and recent developments," Multibody Sys. Dynamics, v1, pp. 189-222, 1997.

[2] Saha, S. K., "Dynamic modeling of serial multibody systems using decoupled natural orthogonal complement matrices," ASME J. of App. Mechanics, v29, No. 2, pp. 986-996, 1999.

[3] Ge, S. S., Lee, T. H. and Zhu, G., "Improving regulation of a single-link flexible manipulator with strain feedback," IEEE Trans. of R. and A, v14, No.1, pp. 179-184, 1998.

[4] Stieber, M. E., McKay, M., Vukovich, G. and Petriu, E., "Vision based sensing and control for robotics applications," IEEE Trans. on Inst. and Meas., v48, No. 4, pp. 807-812, 1999.

[5] Feliu, V., Garcia, A. and Somolinos, J. A., "Gauge-based tip position control of a new three degree of freedom flexible robot," Int. J. of R.R., v20, No. 8, pp. 660-675, 2000.

[6] Mohan, A., Saha, S. K. and Singh, S. P., "Hybrid formulation for robot dynamic models," Proc. of Nat. Conf. on PDMSGQ, Madurai, 2005, pp. 58-65.

[7] Thompson, W., T.,"Theory of Vibrations with Applications," 5th ed., Prentice-Hall, New Jersy, 1998.